Available online at www.sciencedirect.com
SCIENCE DIRECT®
Journal of the European Ceramic Society 25 (2005) 1201–1214
www.elsevier.com/locate/jeurceramsoc

Creep resistance of the directionally solidified ceramic eutectic of Al_2O_3/c-$ZrO_2(Y_2O_3)$: experiments and models

J. Yi [a], A.S. Argon [a,*], A. Sayir [b]

[a] *Massachusetts Institute of Technology, Cambridge, MA 02139, USA*
[b] *NASA-John Glenn Research Center, Cleveland, OH 44135, USA*

Available online 16 February 2005

Abstract

The creep resistance of the directionally solidified ceramic eutectic of Al_2O_3/c-$ZrO_2(Y_2O_3)$ was studied in the temperature range of 1200–1520 °C both exprimentally and by mechanistic dislocation models. The topologically continuous majority phase of Al_2O_3, has a nearly perfect growth texture in the [0 0 0 1] direction and encapsulates the minority c-$ZrO_2(Y_2O_3)$ phase in a variety of morphologies. This encapsulated minority phase too has a close to ⟨1 1 2⟩ growth texture, regardless of morphology. The two phases are separated by close to coherent and well structured interfaces.

The creep of the eutectic in its growth direction exhibits an initial transient that is attributed to stress relaxation in the c-$ZrO_2(Y_2O_3)$ phase, but otherwise in steady state shows many of the same characteristics of creep in sapphire single crystals with *c*-axis orientation. The creep strain rate of the eutectic has stress exponents in the range of 4.5–5.0 and a temperature dependence suggesting a rate mechanism governed by oxygen ion diffusion in the Al_2O_3. While required TEM evidence is still incomplete, finite element analysis of stress distribution in the two phases and a detailed dislocation model of the creep rate indicate that much of the nano-scale encapsulated c-$ZrO_2(Y_2O_3)$ is too small to deform by creep so that the major contribution to the recorded creep strain is derived from the diffusion-controlled climb of pyramidal edge dislocations in the Al_2O_3 phase. The evidence suggests that the climbing dislocations in Al_2O_3 must repeatly circumvent the c-$ZrO_2(Y_2O_3)$ domains acting as dispersoids resulting in the stress exponents larger than 3. The creep model is in very good agreement with the experiments.

Keyword: Al_2O_3/c-ZrO_2 eutectics

1. Introduction

As Fleischer[1] noted, to reach beyond the capabilities of the present set of high temperature superalloys and some intermetallic compounds that have service limitations at around 1000 °C, it is necessary to consider other compounds such as oxides, carbides, borides, etc. to reach service temperatures in the 1400–1600 °C range. While these are all intrinsically brittle materials, having low temperature brittleness problems, their high temperature performance is largely governed by their creep resistance and fracture resistance. It is creep resistance that is of principal concern here to us.

For some time single crystal sapphire fiber with [0 0 0 1] axis orientation has been considered as an ideal material for high temperature application.[2] In that orientation with its principal basal and prismatic systems unstressed, sapphire single crystal fibers have remarkable creep resistance in the 1400–1600 °C temperature range where only the pyramidal slip system is stressed. Early experiments of Firestone and Heuer[3] on [0 0 0 1] axis-oriented-sapphire in the 1600–1800 °C range produced evidence that such sapphire crystals creep entirely by the climb of the 1/3 ⟨$\bar{1}$ 1 0 1⟩ pyramidal edge dislocations, with no slip line or stereo-TEM evidence of glide of such dislocations on any of the possible pyramidal planes available. That such dislocations are entirely sessile in glide has now been established in very recent MD simulations of the core structures of these dislocations.[4,5] The stress dependence of the creep rates of [0 0 0 1] oriented sapphire crystals

* Corresponding author. Tel.: +1 617 253 2217; fax: +1 617 258 8742.
E-mail address: argon@mit.edu (A.S. Argon).

0955-2219/$ – see front matter © 2005 Elsevier Ltd. All rights reserved.
doi:10.1016/j.jeurceramsoc.2005.01.018

and their governing activation energy of oxygen ion diffusion in Al_2O_3 have all been consistent with a pure climb mode of creep.[3] This is extremely rare in the creep of metals, with the only similar occurrence having been reported by Edelin and Pourier[6] in similarly oriented Mg crystals.

While oriented sapphire single crystal fibers have advantageous characteristies and have been considered with diffusion barrier coatings as reinforcing elements in polycrystalline Al_2O_3 matrixes for composite applications,[7,8] the practice has been costly and lacked flexibility. As an alternative to sapphire-fiber-reinforced ceramic composites, a series of directionally solidified ceramic eutectics, consisting largely of an Al_2O_3 component together with compatible stable oxides of ZrO_2 or YAG combine many of the advantages of sapphire fiber with morphological stability at elevated temperatures and relative ease of production. Of these the Al_2O_3, ZrO_2 system eutectic, with additional 4.2 mol% Y_2O_3 modification to create cubic ZrO_2, has received considerable attention.[9] This eutectic has demonstrated some attractive characteristics. In the laser heated float zone (LHFZ)-produced eutectic in the form of fibers or slender rods the Al_2O_3/c-ZrO_2(Y_2O_3)[#1] eutectics possess a sub-micron scale morphology in which the majority Al_2O_3 phase maintains a topologically continuous form with a remarkably tight [0 0 0 1] growth texture.[10,11,14] The c-ZrO_2 phase, in turn, in various morphological shapes ranging from aligned fibers or platelets in either well organized colonies or in less well ordered forms, usually has one narrow dimension in the 0.2 μm range, and is always fully encapsulated in the Al_2O_3 phase. This eutectic has fairly reproducible and reasonably attractive levels of fracture toughness[12] and possesses high quality nearly coherent interfaces.[13]

The eutectics contain significant levels of residual stress at room temperature, resulting from thermal misfit between the component phases. The Al_2O_3 was found to be in a state uniaxial tension parallel to the axis, at a level of 1.0 GPa while the c-ZrO_2 was in some form of multiaxial compression, roughly at the same level.[10] Such residual stresses that decrease in level at elevated temperatures could still be of importance in initial creep response[14] where they, however, should be rapidly relaxed on the onset of steady creep flow.

Here we will be primarily interested in the creep resistance of these Al_2O_3/c-ZrO_2 eutectics in the 1200–1520 °C range.

2. Experimental details

2.1. Material and characterization

The eutectics of Al_2O_3/c-ZrO_2(Y_2O_3) have all been produced by the Laser Heated Float Zone (LHFZ) method at the NASA John Glenn Research Center.[9] Source rods were prepared using 99.999% pure polycrystalline Al_2O_3 powder (CERAC/pure, Ceralox Corp., Tucson, AZ 08676), and 99.999% pure ZrO_2 and Y_2O_3 powders (Alfa Aesar). These powders were blended in acetone for 70 h using high purity Y_2O_3 stabilized ZrO_2. The slurry was dried, mixed again and formed into cylindrical rods using cold isostatic pressing. These rods were then sintered at 1500 °C in air for 4 h. A LHFZ process was used to produce the directional solidification of rods as described previously.[2] These rods were re-used as source rods to produce final samples. The objective of the second solidification was to minimize the entrapment of gases at the liquid solid interface. The directional solidification rate was at 2 mm/min for both processes. The directionally solidified (DS) rods had cross-sectional dimensions roughly in the range of 1–1.5 mm diameter changing from rod to rod but showed only small thickness variations along their 20–22 cm length in any one rod. They were composed of 67% Al_2O_3 and 33% c-ZrO_2 by volume. Random sectioning of the rods always showed a certain residual component of $Y_3Al_5O_{12}$ (YAG) at levels that were considered to be insignificant. More significant, however, was an unavoidable level of porosity along the center line of many samples, often with substantial pore dimensions to constitute super-critical flaws for fracture. These pores always had smooth surfaces indicating they resulted from inadequate wetting during melting and solidification of the initial charge. In a few instances they resulted in fracture during loading of the creep experiments where they were given no further attention other than characterization of the pore sizes and shapes as a feed-back to improve the production process. TEM specimens made from randomly spaced axial and transverse sections were used for electron diffraction to check orientation of components. These, as well as a limited number of X-ray pole figure determinations obtained from surfaces of axial and transverse section of the bars demonstrated that the Al_2O_3 phase had a growth texture of [0 0 0 1] within 2–3 ° parallel to the specimen axis. Wherever prominent three-fold symmetrical colony structures of c-ZrO_2 were observable on transverse sections, there were notable angular differences between the symmetry axes of these colonies indicating the presence of small angle tilt boundaries in the Al_2O_3 (often in the range of 10 °) with tilt axes parallel to the growth axis. Since such tilt boundaries would not be stressed in samples under tension parallel to the bar axis, they were not considered to be of any importance in the creep behavior.

A few direct lattice imaging observations were also made of the structure of interfaces. Fig. 1 shows one such direct lattice image of a typical interface that is incoherent but atomically narrow.

Corresponding determination of the texture of the c-ZrO_2 phase, largely based on electron diffraction information, indicated that this phase had primarily a ⟨1 1 2⟩ growth texture with fiber symmetry, incorporating random rotations about this axis.[#2] The sketch of Fig. 2 shows pictorially

[#1] We note that about 4.2 mol% of Y_2O_3 in the entire eutectic is required to form cubic zirconia. Hereafter in the paper, however, we refer to cubic zirconia merely as c-ZrO_2.

[#2] Textures such as ⟨1 1 1⟩ have also been reported by other investigators.

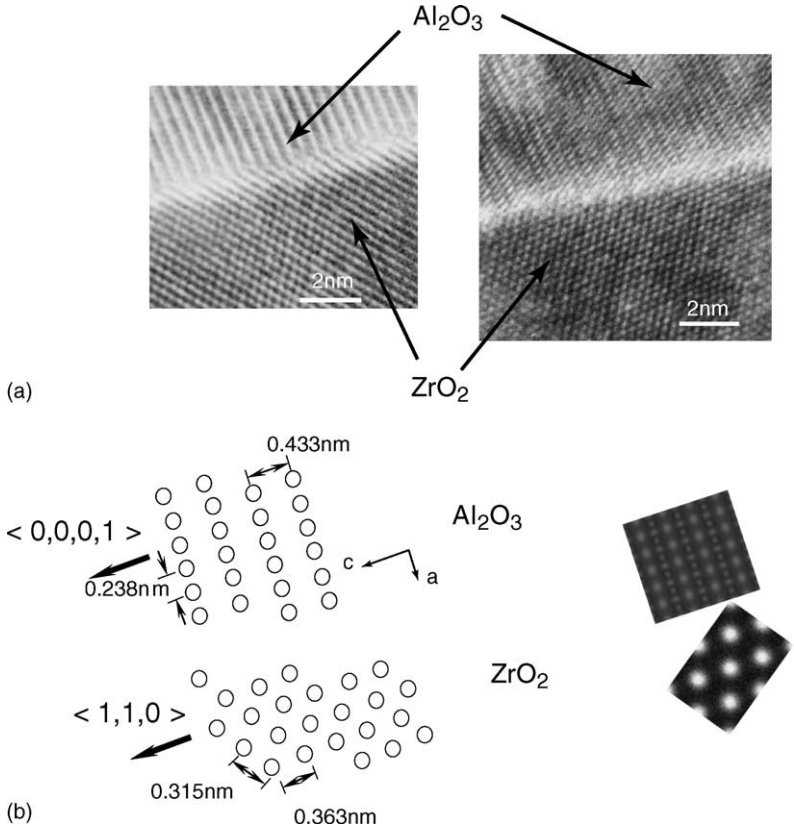

Fig. 1. Direct lattice images of a typical interface between Al_2O_3 and c-ZrO_2 in an Al_2O_3/c-ZrO_2(Y_2O_3) eutectic.

the mutual orientational association of the two component phases.

2.2. Creep equipment and creep strain measurement

The creep experiments were carried out in tension inside a Centorr vacuum chamber containing a specially designed hot zone of 5 cm diameter and 5 cm length made up of a split cylindrical configuration of a 1 mm thick Ta sheet with alternating up-and-down slits to increase the path length of the heating element. The hot zone was surrounded by a series of Mo radiation shields. The long specimens threaded through the hot zone and were gripped at their ends by specially produced metallic friction grips, clamping down on the ends of the specimens through annealed soft nickel sheets to avoid high local contact forces on the rods that could have resulted in fracture. Two relatively massive water cooled OFHC Cu plates were placed between the two exits of the hot zone and the specimen grips to assure that the gripping conditions were, as much as possible, at low temperature not to exceed about 200 °C to avoid slippage in the grips. Stressing of specimens was by externally applied deadloads.

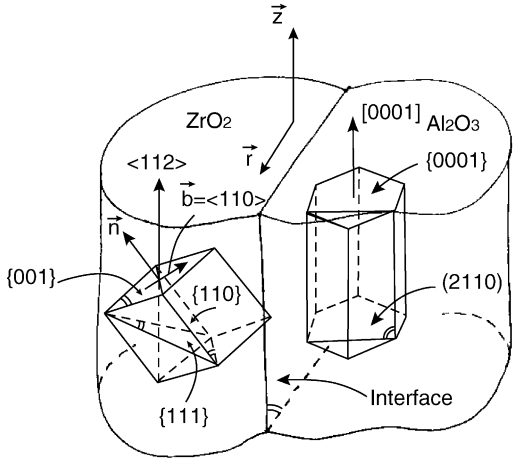

Fig. 2. Sketch showing the textural arrangement of the Al_2O_3 component with a preferred [0 0 0 1] axis and c-ZrO_2 with a preferred ⟨1 1 2⟩ axis found by electron diffraction analysis. Other textures for c-ZrO_2 have also been reported.

An optical grade sapphire window permitted viewing the hot specimen through a narrow axial slit in the heating elements to permit direct measurements of the specimen temperature by means of a two-wave-length pyrometer (from Omega Vanzetti, Sharon, MA, USA), providing emissivity-independent measurements. In addition to a control thermocouple inside the hot zone, another thermocouple placed close to the specimen without touching it, was used to actually record the steady temperature in the thermal cavity. The temperature measured by this second thermocouple and that measured by the pyrometer on the specimen usually

agreed quite well. The hot zone temperature was automatically controlled by the PID control system of the Centorr equipment.

Since the steady state creep extensions of the specimens under stress were generally quite small, to eliminate random flexures and motions of the massive creep frame from influencing the measurements, the displacements of the two ends of the load train immediately outside the vacuum chamber were simultaneously measured by sets of four LVDTs at both the top and bottom ends of the Centorr chamber. The differences between these two measurements then corresponded to the extension of the specimen. Since the temperature of the specimen inside the hot zone was higher by 1200–1300 °C above the portions of the sample outside the hot zone, the gauge length was taken as the axial extent of the hot zone. Even under ideal conditions the total creep strain was never too uniquely determinable. To overcome this difficulty all creep strains at steady state were always measured incrementally at a given temperature under two different applied stresses and often as loading and unloading cycles. This practice of relative measurements of creep strain did not only give more reliable determinations of the strain rates at the two different levels of stress but also demonstrated the nearly complete absence of transients in such incremental changes in steady state creep. A typical response of this type is shown in Fig. 3 for creep at 1520 °C at stress levels of 150 and 200 MPa. The random-appearing irregularities on the creep curves in Fig. 3 were attributed to be of instrumental origin. When determining actual increments of creep strain in any interval of time these variations were operationally smoothed out. The accuracy of strain measurement was around 1.4×10^{-5}.

3. Experimental results

3.1. Transient effects

Upon initial application of stress to a virgin specimen a strain transient was always observed. One such transient recorded for an experiment at 1200 °C under a stress of 300 MPa is shown in Fig. 4. The characteristic time constant of the transient decreased with increasing temperature, e.g. from ca. 3.4×10^3 s at 1200 °C to 200 s at 1400 °C. The usual explanation of the transient to be due to initial work hardening in the creeping components prior to establishment of a steady state by recovery processes, familiar in creep of homogeneous metals, was discounted here since no prominent transients were found following stress increases at steady state creep. The most likely cause of the transient was the rapid stress relaxation in the coarse c-ZrO_2 component by creep since for the measured texture of that component there is an abundance of the ⟨1 1 0⟩{1 0 0} principal slip systems that are well oriented for slip, and the creep resistance of c-ZrO_2 in this temperature range is known to be poor.[15] In more ideal morphologies, as presented by Sayir and Farmer[2] and Argon et al.,[17] the coarse fraction of the c-ZrO_2 is located on colony borders. In the usual less ideal morphologies where fibrillar c-ZrO_2 is still aggregated but does not form well-structured colonies the coarse fraction was found to be less regularly distributed (see Fig. 7). An upper bound manifestation of the poor creep resistance of c-ZrO_2 can be assessed from a finite element (FEM) study that will be presented in Section 4.3. There it was found that for the complete relaxation of the deviatoric stresses in the entire c-ZrO_2 phase the volume average deviatoric stresses as well as mean normal stresses in the Al_2O_3, increase roughly by 25–30% which would result in an increment of additional elastic strain in the sample of about 6×10^{-4}. This level is illustrated in Fig. 4

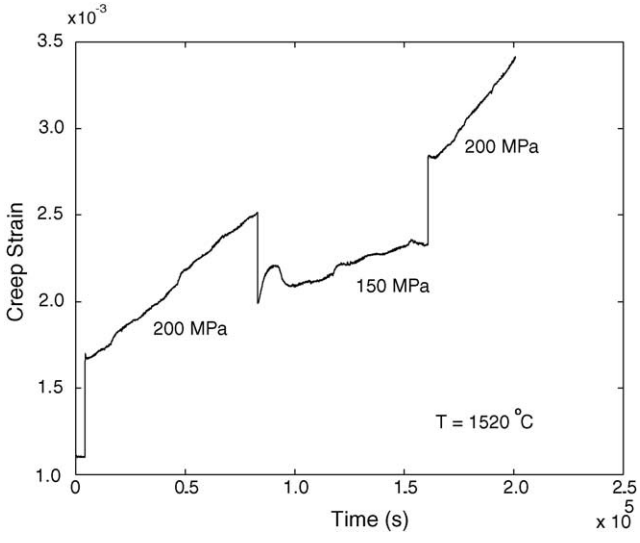

Fig. 3. A typical strain time plot for steady state creep at two different stress levels in an Al_2O_3/c-ZrO_2 eutectic rod at 1520 °C.

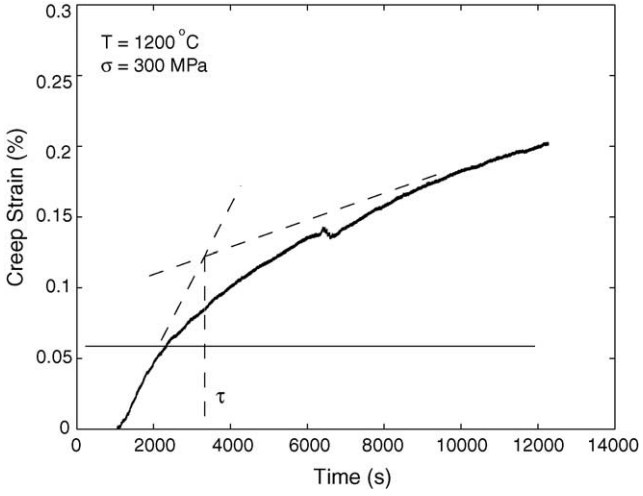

Fig. 4. A typical creep strain transient in an Al_2O_3/c-ZrO_2 eutectic under a stress of 200 MPa at a temperature of 1200 °C. The horizontal line gives an estimate of creep strain increment due to stress relaxation in the coarse fraction of c-ZrO_2.

Table 1
Recorded steady state strain rates

Stress (MPa)	Strain rate $\dot{\varepsilon}$(sample #)[$\bar{\dot{\varepsilon}}$ average rate] (s^{-1})
1200 °C	
200	1.97×10^{-10} (142-18)
1400 °C	
200	3.6×10^{-9} (187-29)
225	2.26×10^{-9} (187-27-2); 8.16×10^{-9} (187-27-1) [5.21×10^{-9}]
250	5.53×10^{-9} (187-29)
275	9.95×10^{-9} (187-27-2); 1.10×10^{-8} (187-27-1) [1.048×10^{-8}]
1520 °C	
150	1.57×10^{-9} (142-16); 4.40×10^{-9} (142-16) [2.98×10^{-9}]
200	1.20×10^{-8} (142-16); 1.60×10^{-8} (142-16) [1.40×10^{-8}]

by the horizontal line. The actual amount of stress relaxation in the c-ZrO_2, however, is difficult to determine since a substantial fraction of this component has phase dimensions in the range of 0.2–0.4 μm and is likely to be dislocation-free and incapable of plastically deforming as we discuss in Section 4. These, and the difficulties in determining the absolute measures of strain derived from the hot zone portions of the samples requires us to de-emphasize this portion of the creep response.

3.2. Steady state creep

As already mentioned in Section 2.2 the main information on steady state creep was obtained from incremental experiments of sudden stress increases and decreases at constant temperature as shown in the typical case of Fig. 3 of creep response. A simple check of the magnitude of the instantaneous stretches or contractions for stress increases or decreases, utilizing the appropriate information on the temperature dependent Young's modulus of Al_2O_3[16] gave in all cases that the recorded jumps were all about a factor of 2 larger than what could be expected from the sample in the hot zone. Since this was well within the additional flexures and relaxations in the load train the recorded strain rates were considered to be reliable.

After the final configuration of the hot zone discussed in Section 2.2 was completed, 11 determinations of steady state creep rate were made, all together at 3 temperatures of 1200, 1400, 1520 °C at stress levels ranging from 150 to 275 MPa, derived from incremental experiments similar to those in Fig. 3. These measurements are listed in Table 1 and are plotted in Fig. 5 together with the creep rates at 1400 °C due to Sayir and Farmer.[2,17,#3] The stress exponents of the

[#3] The higher creep rates and the larger stress exponents in these early investigations are most likely a result of not reaching steady state but still being in a late stage of transient behavior.

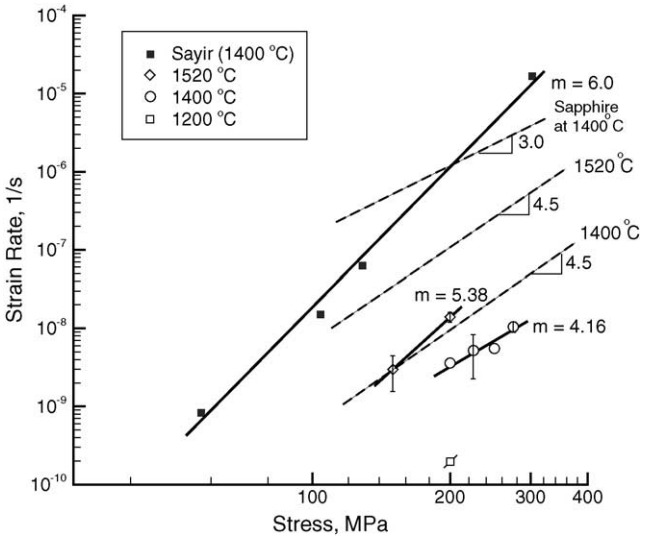

Fig. 5. Plots of steady state creep rates as a function of stress for temperatures of 1200, 1400 and 1520 °C compared with measurements reported by Sayir and Farmer.[2] Broken lines represent predictions of creep model for Al_2O_3/c-ZrO_2 at 1400 and 1520 °C, together with model prediction for sapphire at 1400 °C.

creep rates at 1400 and 1520 °C, shown in Fig. 5, are 4.16 and 5.38 and are lower than that of Sayir at 6.00. As we will discuss in the creep model in Section 4.3, these exponents are relatively high and need to be explained, as we will do later in Section 4.4.

Table 1 contains also sufficient information for the determination of the activation energy of the governing creep process. The plot of the creep rates at a stress of 200 MPa for three temperatures of 1200, 1400 and 1520 °C in Fig. 6 gives an activation energy of $Q = 71.1$ kcal/mol for the rate controlling

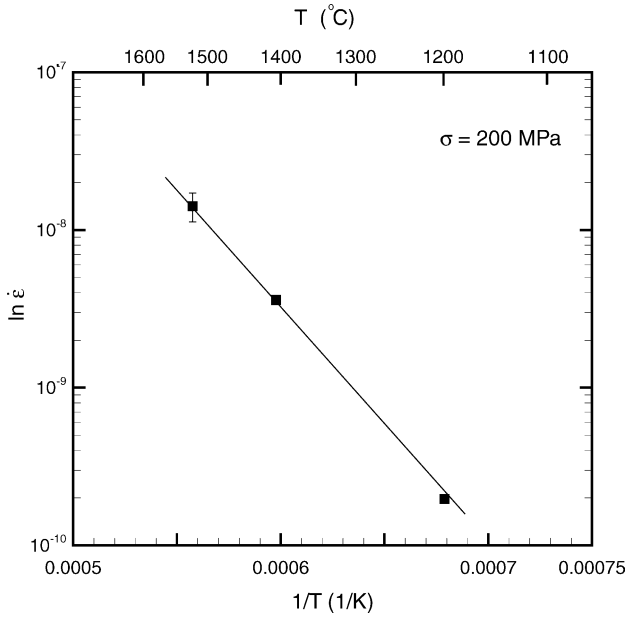

Fig. 6. Determination of activation energy of steady state creep from temperature dependence of steady state creep rate.

process in steady state creep which we consider to be due to oxygen ion diffusion which is known to be the slowest species in Al_2O_3. This value is to be compared with 105 kcal/mol for temperatures above 1400 °C and 26 kcal/mol for temperatures below 1400 °C for the same process measured by Oishi and Kingery[25] in pure polycrystalline Al_2O_3. The somewhat lower magnitude of the measured activation energy for oxygen ion diffusion is attributed to the likelihood that a significant fraction of the diffusion current will be along the the incoherent interfaces.

4. The creep model

4.1. Basic assumptions

The fact that the c-ZrO_2 of considerably lower creep resistance is encapsulated everywhere by the topologically continuous Al_2O_3 with a very tight growth texture of [0 0 0 1] along the axes of the DS eutectic rods indicates that steady state creep must be controlled by the Al_2O_3 phase, once any limited compliance increment due to the stress relaxation in the coarse fraction of c-ZrO_2 is complete. This suggests that the overall creep response must have the same characteristics of steady state creep in sapphire single crystals reported by Firestone and Heuer,[3] albeit with certain important added complexities derived from the presence of the c-ZrO_2 phase. Fig. 7 shows the well-known phase morphology of a typical Al_2O_3/c-ZrO_2 eutectic where the bright phase is the c-ZrO_2. Very much like the γ' phase in superalloy single crystals of CMSX-3,[18] a large fraction of the c-ZrO_2 has dimensions in the range of 0.2–0.4 μm and must be regarded as being too small to have the capability of undergoing plastic flow by independent internal processes of dislocation multiplication by glide or climb, as already remarked above. The c-ZrO_2 phase components of larger dimensions, as the irregular shaped ones in Fig. 7 should undergo rapid stress relaxation in the 1200–1520 °C temperature range of interest, as the transient creep curve of Fig. 4 suggests. Such stress relaxation by glide on the $\{1\,0\,0\}\langle 1\,1\,0\rangle$ primary systems in the c-ZrO_2 component having a $\langle 1\,1\,2\rangle$ texture should be relatively unhindered. Even so, as we present in Section 4.3, FEM analysis shows that complete shear stress relaxation in the c-ZrO_2 still leaves the mean normal stress intact in it which prevents large average stress enhancement in the Al_2O_3 phase.

Since the best slip systems of the basal and prismatic type are largely unstressed for glide due to the tight texture of the Al_2O_3 phase, and since the pyramidal dislocations of $1/3\langle 11\bar{2}\,0\,1\rangle$ type are sessile in glide, due to a unique core restructuring process as has been recently demonstrated,[4,5] we expect that creep in this component for eutectic fibers in tension, can only be a consequence of climb of the $(1/3)\langle 11\bar{2}\,0\,1\rangle$ dislocations, whether they exist on the prism planes or on the pyramidal planes. This has already been recognized by Firestone and Heuer.[3] Creep, derived entirely from climbing edge dislocations is quite rare in structural metals. The only previously reported similar case is in Mg single crystals stressed in the [0 0 0 1] direction.[6] Nabarro[19] has presented an idealized model of creep derived from climb of a Frank type dislocation network where material fluxes are between the actual climbing dislocations with Burgers vectors parallel to the stress axis and those of other types experiencing no climb forces. Firestone and Heuer[3] found rea-

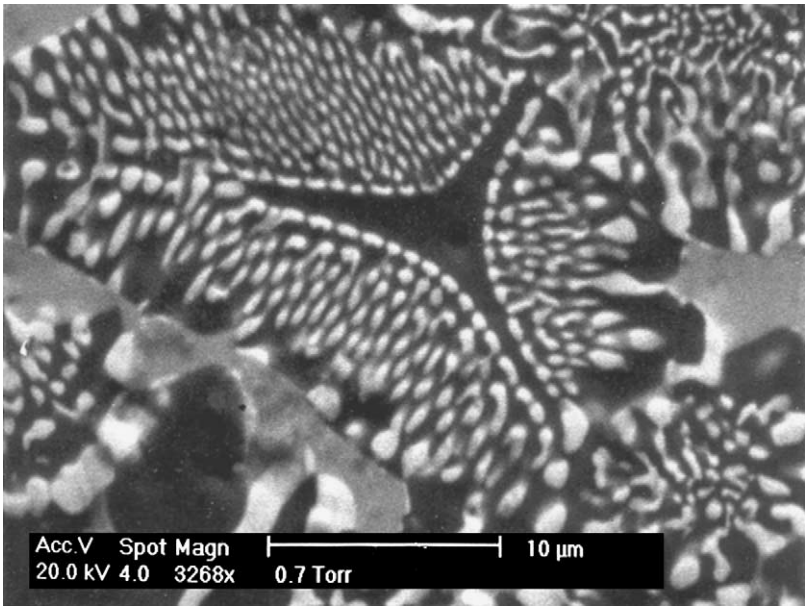

Fig. 7. An SEM micrograph of a typical morphology of the Al_2O_3/c-ZrO_2 eutectic, as revealed in a transverse section. The phase morphology of the longitudinal section, while somewhat different, is statistically quite similar to that of the transverse section. The black component is Al_2O_3. Much of the c-ZrO_2 component (the bright regions) is of low sub-micron size and is expected not to deform by any form of crystal plasticity.

sonable agreement of their results where the stress exponents were in the range of 3 as the Nabarro model predicts. In our case where the stress exponents are in the range of 4.5–6.0 we expect different conditions to hold, requiring considerable modification of the Nabarro framework.

Since basic TEM information is still largely absent to furnish better guidance, in our model, we make a number of essential assumptions. We assume that the $(1/3)\langle\bar{1}1\,0\,1\rangle$ dislocations pre-exist in the Al_2O_3 phase, having been generated during the directional solidification process while the morphology is being established, and will multiply by topological convolution processes in well known ways from sources, and will be available for climb under stress during creep. We expect that the mean free path lengths of climbing dislocations in Al_2O_3 will involve several multiples of the interphase dimensions, i.e. be of the order of microns, requiring the climbing dislocations to repeatedly bow and straighten-out as they thread through the small c-ZrO_2 domains that will remain impenetrable to them. Such repetition of transient line shapes will be viewed as the primary source of the elevation of the creep stress exponents to become larger than 3.[20] We assume that the climbing pyramidal dislocations can multiply by topological process a'la Bardeen and Herring.[21] As for the climb of these dislocations, we assume that this will be diffusion controlled with adequate jog concentrations present along the dislocations, these we expect to be produced by nodal emission processes from network junctions rather than being of a thermal equilibrium nature which preliminary analyses show to be far too difficult. We assume that the diffusional transport will be between dislocation cores and the large concentrations of incoherent or semi-coherent interfaces. We assume also that the interfaces will be completely opaque to the transmission of dislocations from c-ZrO_2 to Al_2O_3 or vice versa. Analysis indicates that such transmission would be subject to extremely large energy barriers, that can not be overcome. We expect that the residual stresses due to initial thermal misfit between the components will be relieved during the transient phases of the creep and provide another contribution to the recorded amounts shown in Fig. 4, but that steady state creep will be governed by the climb forces resulting entirely from the applied stress.

Finally, we expect that as the topologically continuous framework of the Al_2O_3 creeps and extends, while the c-ZrO_2 largely remains either dormant or is merely stress-relaxed, global back stresses will develop in the Al_2O_3, gradually slowing down the creep rate.[22] Since the creep ductilities of the eutectics are quite modest, we do not expect this back stress to develop fast enough to be of consequence, and ignore it.

4.2. The creep rate

Consider a round tensile creep bar of an Al_2O_3/c-ZrO_2 eutectic as sketched in Fig. 8 where local axes 1, 2, 3, are chosen in a pyramidal glide system with axis 1 chosen parallel to the $1/3\langle\bar{1}1\,0\,1\rangle$ Burgers vector, axis 2 normal to the pyramidal plane making an angle φ with the bar axis, and axis 3 parallel to the line vector of a positive edge dislocation. Under a uniform stress σ_1 a positive edge dislocation will climb in the negative 2 direction with a velocity v_c to contribute to a uniaxial tensile creep strain rate parallel to the 1 direction. This velocity, if it were governed by diffusion controlled climb would be given by Friedel[23]:

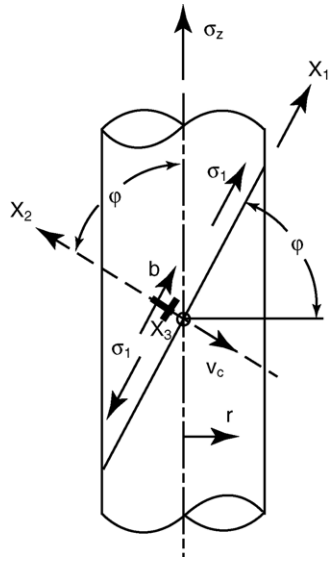

Fig. 8. Sketch of a round bar of a Al_2O_3/c-ZrO_2 eutectic with z-axis parallel to the [0 0 0 1] direction of the Al_2O_3. The plane at angle ϕ outlines a pyramidal glide plane. A local tensile stress σ_1 will make a positive edge dislocation climb in the negative X_2-direction.

$$v_c = \frac{2\pi D(\sigma_1 - \sigma_T)b^2}{kT\ \ln(r_s/r_c)} \tag{1}$$

where $D = D_0 \exp(-Q/RT)$ is the diffusion constant of Al_2O_3 where oxygen is recognized to be the slow diffusing species, σ_T is the triaxial component of the applied stress ($\sigma_z/3$) that does not promote equilibrium climb, r_s is the distance from the dislocation core to vacancy sinks along the interfaces, r_c the core radius from which point defect emission is considered, b the magnitude of the Burgers vector, D_0 the pre-exponential factor of the diffusion constant, Q the activation energy of O ion diffusion in Al_2O_3 and R and T have their usual meaning. The kinematics of shape change due to climb alone of dislocations has been considered more broadly by Groves and Kelly.[24] In our case a more specialized consideration will be adequate. Thus, considering that there will be three equivalent pyramidal systems that can contribute to the axial strain rate equally, as is explained in the Appendix A, the axial creep strain rate $\dot{\varepsilon}_z$ along the bar and the accompanying radial contractile strain rates $\dot{\varepsilon}_r$ are given respectively as:

$$\dot{\varepsilon}_z = (2 - 3\cos^2\phi)\dot{\varepsilon}_0 \tag{2a}$$

and

$$\dot{\varepsilon}_r = -\left(1 - \frac{3}{2}\cos^2\phi\right)\dot{\varepsilon}_0 \tag{2b}$$

where

$$\dot{\varepsilon}_0 = b\rho_m v_c \tag{3}$$

is the main creep rate in the pyramidal system coordinates without regard to overall volume preservation , which is considered to result in Eqs. (2) and (3) (see Appendix A). Relating the actual climb-producing tensile stress σ_1 to the axial stress σ_z and considering the volume-average effect of the local variation of stress due to the presence of the c-ZrO_2 components by a factor q we have

$$\sigma_1 - \sigma_T = \frac{2}{3}q\sigma_z(1 - cos^2\phi) \tag{4}$$

If the mobile dislocation density, ρ_m, of climbing dislocations at steady state is governed by mutual interactions in a self adjusting basis[19]; i.e.

$$\rho_m \cong \left(\frac{2\pi\sigma_z}{\mu b}\right)^2 q^2(1 - \cos^2\phi)^2 \tag{5}$$

we have, by finally combining Eqs. (2), (4), (5) and (6) the axial steady state creep rate:

$$\dot{\varepsilon}_z = A\left(\frac{D}{b^2}\right)\left(\frac{\sigma_z}{\mu}\right)^3\left(\frac{\mu\Omega}{kT}\right)\frac{(1 - \cos^2\phi)^3(2 - 3\cos^2\phi)}{\ln(r_s/r_c)} \tag{6}$$

where

$$A = \frac{2}{3}(2\pi)^3\frac{q^3}{\beta} \tag{7a}$$

and

$$\beta = \Omega/b^3 = 0.079 \tag{7b}$$

where Ω is the ionic volume of O in the Al_2O_3 lattice and q is a factor which relates the local volume average climb stress to the axial stress σ_z as is determined from a FEM analysis of the stress distribution in the Al_2O_3 phase under an applied tensile stress as discussed in Section 4.3 (Fig. 9).

Eq. (7) gives the creep rate due to the climb of quasi-straight dislocations in a homogeneous stress field. As we discuss in Section 4.4 this is not the case in the Al_2O_3/c-ZrO_2 eutectics where the climbing dislocations need to thread through the non-deforming c-ZrO_2 domains acting as dispersoids and are required to alternately bow around these domains and be released to straighten out, acting effectively as if straight dislocations were moving through a strongly varying internal stress field which will increase the stress exponent in predictable ways and decrease the actual creep rate.[20]

In Section 4.5 we will evaluate the creep model and compare it with the experimental results.

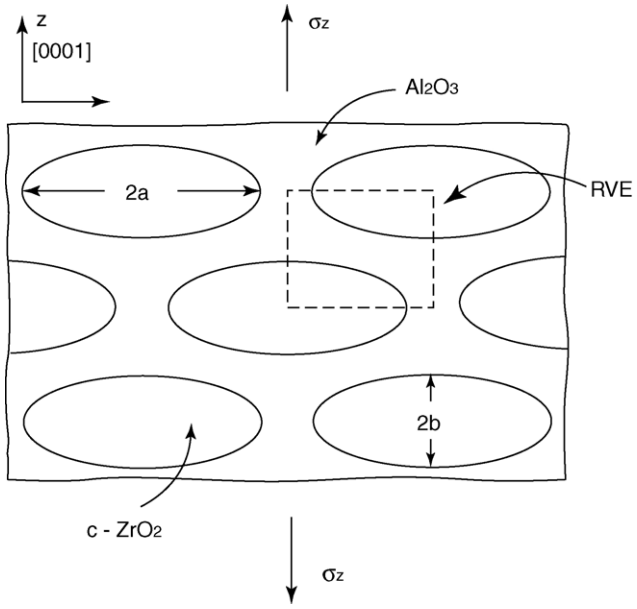

Fig. 9. Sketches of an idealization of the c-ZrO_2 domains as ellipsoidal cylinders in the topologically continuous Al_2O_3 component, for the purpose of a FEM study of the internal stress distribution in the Al_2O_3 when a tensile stress σ_z is applied.

4.3. Distribution of stresses in the Al_2O_3/c-ZrO_2 eutectics

A very important way in which creep in the eutectics differs from creep in single crystal sapphire is that in the former the stresses are distributed in a complex manner. In addition to residual stresses arising from the different thermal expansions of the two components, the applied stresses result in complex internal local stress distributions due to different elastic properties of the Al_2O_3 and the c-ZrO_2 component phases. Thus, to develop some necessary understanding of this phenomenon on a broad basis, a linear-elastic FEM analysis was carried out in a 2-D plane strain setting of the eutectic in the ordered regions shown in Fig. 7. Here the c-ZrO_2 domains in 2-D are taken as elliptical cylinders occupying a volume fraction of 0.33. The chosen representative computational volume is indicated in this figure. We have considered the c-ZrO_2 to be always fully relaxed of all shear stresses but with an unrelaxed appropriate bulk modulus of 83 GPa. This is accomplished operationally in the FEM code for purely elastic behavior by choosing the Young's modulus of the c-ZrO_2 as 0.05 MPa and the Poisson's ratio as 0.4999999. All other chosen material constants are listed in Table 2. In the broader analysis we considered the aspect ratios of ellipsoidal rods, a/b of c-ZrO_2 as 1, 3, 4 and 5. Of these results we present here only the distributions for $a/b = 3.0$ as most representative. All analyses were limited to the elastic range. In this FEM framework we considered several process simulations: (a) an applied tensile stress σ_z alone; (b) cooling the morphology from a stress-free condition at 1875 °C down

Table 2
Material properties for linear elastic FEM analysis

	Al_2O_3	c-ZrO_2
Young's modulus	190 GPa at 1400 °C	0.05 MPa at 1400 °C[a]
Poisson's ratio	0.3	0.4999999[a]
Yield stress	5.0 GPa[b]	5.0 GPa
Coefficient of thermal expansion ($°C^{-1}$)	9.1×10^{-6} (a) 9.9×10^{-6} (c)[14]	12.9×10^{-6} [14]

[a] These values were chosen in the FEM code result in a negligible shear modulus for c-ZrO_2 to obtain a state of near complete shear relaxation while leaving the bulk behavior intact.
[b] These high yield stresses were chosen in the FEM code to guarantee pure elastic response.

to 1400 °C to determine residual stresses and; (c) cooling as in (b) plus an applied tensile stress of $\sigma_z = 300$ MPa. Of these, we discuss here only the case of the internal stress distribution under an applied stress $\sigma_z = 300$ MPa (since behavior is linear-elastic, results for all other stress levels can be determined by re-scaling).

In Fig. 10a we show the distribution of the Mises deviatoric stresses for the case of $\sigma_z = 300$ MPa and $T = 1400\,°C$, in the Al_2O_3 region. As expected, the states of stress inside the ellipsoidal regions of the c-ZrO_2 are close to constant. Fig. 10b gives the more important distribution of the climb stress σ_1, parallel to the pyramidal dislocation Burgers vector at an angle of $\phi = 57.7°$ as shown in Fig. 8. The volume-average level of this important climb producing stress was found to be $\sigma_1 = 216.3$ MPa which gives the factor q to be 0.721. This value appears surprisingly low in view of the assumed complete relaxation of the deviatoric stresses in the c-ZrO_2, until it is recognized that the c-ZrO_2 still supports fully a mean normal stress which limits the stress enhancement in the Al_2O_3 component.

4.4. Effect of internal resistance variations

As stated in Section 4.2 the creep response of the Al_2O_3/c-ZrO_2 eutectics differ significantly from the creep behavior in homogeneous sapphire single crystals studied by Firestone and Heuer.[3] First because of the non-uniform stress distribution in the morphology of Al_2O_3 and c-ZrO_2 discussed in Section 4.3 above but even more importantly by the large perturbations that the climbing dislocations encounter threading through the isolated and largely non-deforming c-ZrO_2 domains. Thus, consider the convolutions that a climbing dislocation has to go through as it threads through the gaps of the c-ZrO_2 domains as depicted in Fig. 11. First, the climbing dislocation must squeeze into the gaps between the domains as depicted in Fig. 11a to a critical configuration much like the Orowan bowing process for non-shearable dispersoids. The peak stress that is required for this configuration to be achieved is

$$\sigma = \sigma_i = \frac{2\mathcal{E}}{b\Lambda} = \frac{\mu b}{\Lambda} \tag{8}$$

where $\mathcal{E}$ is the dislocation line tension ($\mu b^2/2$) and Λ is the size of the inter-domain gap. Clearly, here the process is not one of glide but climb where σ is the climb stress. Once the critical configuration is reached and the climbing dislocation surrounds the impenetrable domain and pinches off as shown in Fig. 11b, the separated dislocation has acquired a definite cusp where this shape of the dislocation will undergo accelerated climb due to the advantageous line tension effects. We view these required contortions of the dislocations as if they were the same as positive and negative internal stresses σ_i, retarding and then accelerating climb, very much like the corresponding cases of favorable and unfavorable internal stresses that a glide dislocation needs to go through between dispersoids. Such problems were treated in great detail by many investigators, but particularly thoroughly by Li,[20] which illustrated that a gliding dislocation (in our case a climbing dislocation) loses more time in the region of adverse internal stress than the time it gains in moving through regions of favorable internal stress. The effect is illustrated in Fig. 12, where 12a shows the sinusoidally varying internal stress σ_i and the prevailing climb stress σ. The most important consequence of such deceleration and acceleration of motion is an increase in the effective stress exponent m of the dislocation velocity, scaled by the ratio of σ_i/σ is shown in Fig. 12b. A secondary effect is a factor $C = \overline{v}/v$ that gives the decrease in the average dislocation velocity relative to the velocity in unhindered climb shown in Fig. 12c, also scaled with the ratio of σ_i/σ. To assess a measure of the effect we note from Fig. 7 that in much of the morphology the inter-domain distance Λ would appear to be between 0.3 and 1.0 μm. Taking the small dimension to determine the maximum level of this effect, together with $b = 5.12 \times 10^{-10}$ m and $\mu = E/2(1+\nu) = 73$ GPa[16] at 1400 °C we determine $\sigma_i = 125$ MPa. This, for an applied stress $\sigma_z = 300$ MPa, in the range of interest, that would give a volume average climb stress $\sigma = q\sigma_z(1 - \cos^2\phi)$ of 153 MPa, and a ratio $\sigma_i/\sigma \approx 0.815$, Fig. 12b indicates that the effective stress exponent of the stress in the velocity expression should increase to nearly $m = 3$ from unity as the maximum effect. Moreover, Fig. 12c gives $C = \overline{v}/v = 0.6$. Clearly, larger distances Λ should result in smaller effective internal stresses while smaller applied stresses should give increased ratios σ_i/σ. The overall net effect will be rather complex to assess. Here, we consider that under the conditions described the net effect on the overall stress exponent of the creep rate will be to elevate it from $n = 3$ for the model presented above to $n = (m+2) = (2.5+2) = 4.5$ to $n = (3+2) = 5$. This consideration and the factor C, when

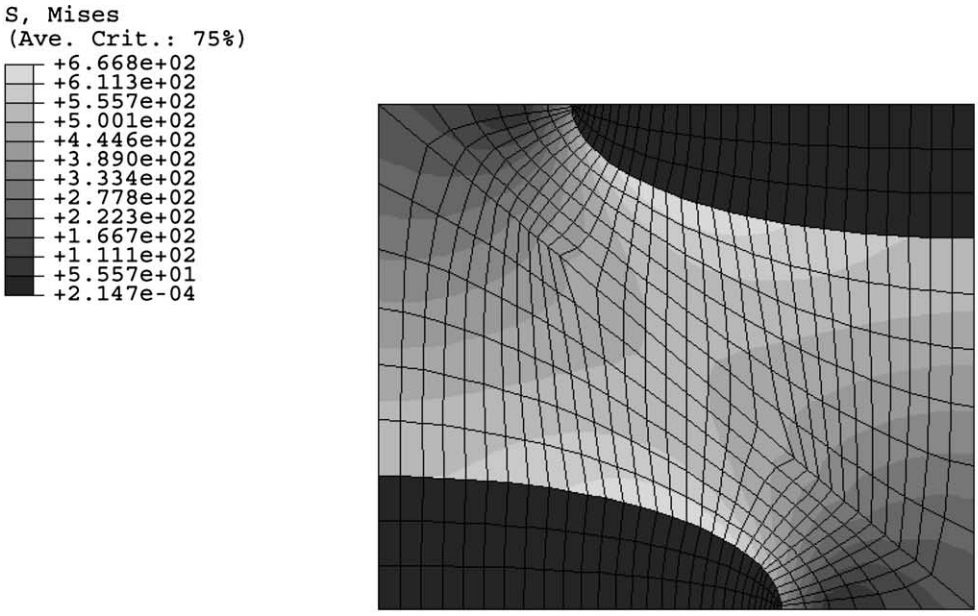

(a)

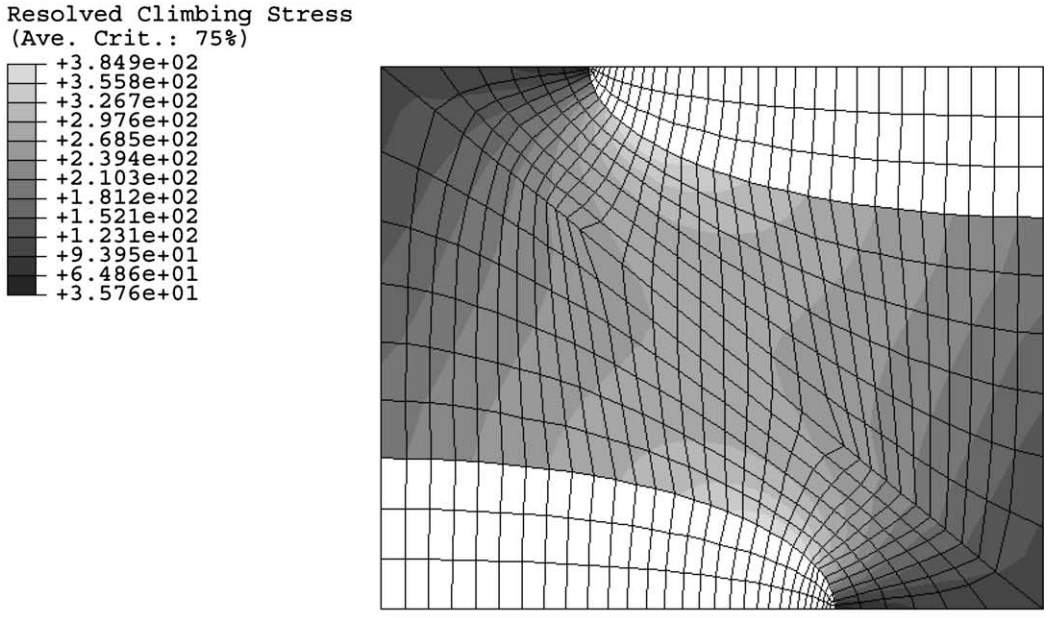

(b)

Fig. 10. Stress distribution results of the FEM study: (a) deviatoric (Mises) stresses in the two components of the eutectic and (b) the distribution of the climb stress σ_1 in the Al_2O_3.

incorporated into the creep model of smooth climb given by Eq. (7) will change it finally to

$$\dot{\varepsilon} = AC\left(\frac{D}{b^2}\right)\left(\frac{\sigma_z}{\mu}\right)^n\left(\frac{\mu\Omega}{kT}\right)\frac{(1-\cos^2\phi)^3(2-3\cos^2\phi)}{\ln(r_s/r_c)} \quad (9)$$

It is this expression that we will compare with the experimental results in Section 4.5.

4.5. Evaluation of the creep model

We now proceed to evaluate our final creep model of Eq. (9) and compare it with experimental results. In the comparison we will evaluate the expression for both 1400 and 1520 °C. We use the following model parameters and material properties:

$\mu = \frac{E}{2(1+\nu)} = 73$ GPa at 1400 °C and 63.4 GPa at 1520 °C[16]

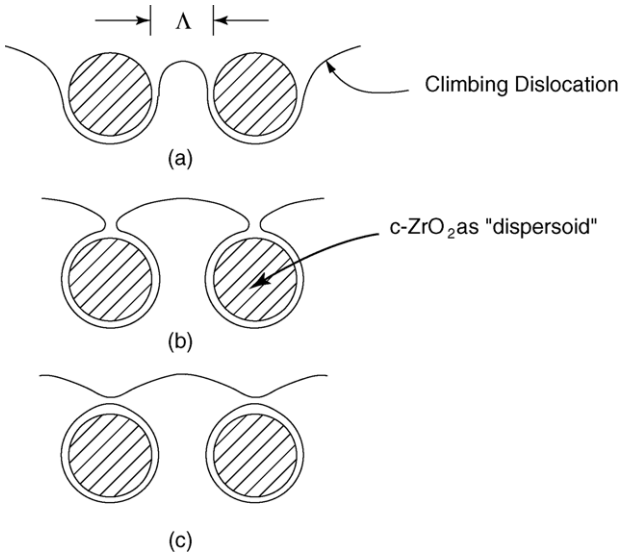

Fig. 11. Sketch depicting the required contortions that a climbing edge dislocation need to suffer in bowing through the gaps between the c-ZrO_2 domains that we consider to be impenetrable: (a) critical climb configuration to bow through the gap between two c-ZrO_2 dispersoids at a spacing Λ, (b) at the point when the climbing dislocation is just about to pinch off, and (c) the cusped dislocation line straightening out under the application of line tension.

$b = 5.12 \times 10^{-10}$m
$\Omega = 1.06 \times 10^{-29}$ m^3
$q = 0.721$ as determined in Section 4.3
$\beta = \Omega/b^3 = 0.079$
$A = \frac{2}{3}(2\pi)^3(q^3/\beta) = 7.85 \times 10^2$
$\phi = 57.7^\circ$
$r_s = 0.5$–2.0 μm, as estimated from micrographs (Fig. 7)
$r_c \approx b$

$D = 10^{-14}$ cm^2/s at 1400 °C and 9×10^{-14} cm^2/s at 1520 °C determined from Oishi and Kingery directly for their polycrystalline material[25] for which, parenthetically the activation energy was $Q = 110$ kcal/mol, considerably larger than our value.

Finally, we take $n = 4.5$ as suggested from our analysis in Section 4.4 above, and

$C = 0.6$.

The calculated steady state creep rate relations for 1400 and 1520 °C are presented in Fig. 5 as the broken lines in comparison with the experimental data.

Considering the several uncertainties in the model and material parameters the agreement between model and experimental results is pleasing.

5. Discussion

The experimental measurements of steady state creep rates in the Al_2O_3/c-ZrO_2 eutectic, while few, have given a good measure of the response of this material in the temperature

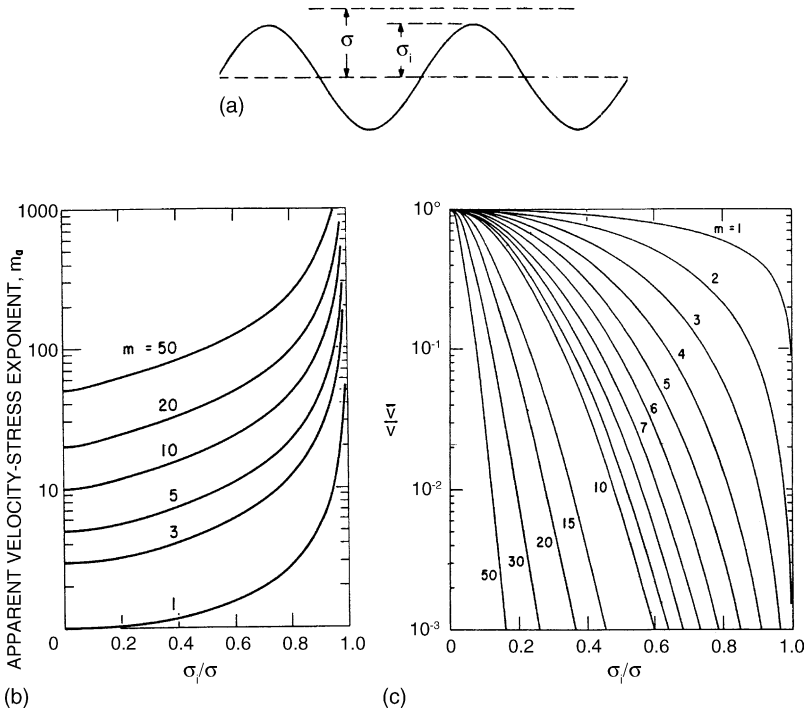

Fig. 12. Consequence of the repeated bowing out and straightening of the climbing dislocation considered as a set of internal resistances σ_i alternately retarding and speeding up the climbing dislocation: (a) retardation and speeding up considered as unfavorable and favorable internal stresses σ_i in the presence of a climb stress σ, (b) effect of σ_i/σ on the overall stress exponent m of the dislocation velocity, and (c) effect of σ_i/σ on the attenuation factor C on the average climb velocity (figures reproduced from Li,[20] courtesy of John Wiley & Sons).

range of interest. Taking account of the possible interactions of the c-ZrO_2 phase with the Al_2O_3 we have developed a steady state creep model based on climb of pyramidal edge dislocations in Al_2O_3 alone. In our model we propose that the c-ZrO_2 phase of relatively large size, in the micron range will most likely undergo nearly complete stress relaxation in the 1400 °C range, resulting in an initial transient creep with relatively short time constant of roughly 200 s.[2] On the other hand the sub-micron size domains of the c-ZrO_2 will most likely be too small to undergo independent deformation processes by crystal plasticity and will remain non-deformable to impede the climb motion of the pyramidal system dislocations in the Al_2O_3 much like dispersoids. The observed creep rate stress exponents in the range of 4–5 are indicative of this behavior. In this sense it would appear that the eutectic through its unique morphology should be more creep resistant than sapphire of [0 0 0 1] axis orientation. To explore this comparison we interpret our creep model for application to sapphire in which the climb motion of the dislocations is expected to be quasi-smooth. Such a modification would give a steady state creep expression of

$$\dot{\varepsilon}_{\text{sap}} = A' \left(\frac{D'}{b^2}\right)\left(\frac{\sigma_z}{\mu}\right)^3 \left(\frac{\mu\Omega}{kT}\right) \times \frac{(1-\cos^2\phi)^3(2-3\cos^2\phi)}{\ln(r_s/r_c)} \quad (10)$$

where $A' = \frac{2}{3}(2\pi)^3/\beta = 2.09 \times 10^3$ (for $q = 1.0$) and D', the diffusion constant, must be chosen for sapphire single crystals not having the benefit of diffusion short circuits along interfaces. From Oishi and Kingery[25] we obtain $D' = 3.5 \times 10^{-17}\,\text{cm}^2/\text{s}$ at 1400 °C, or a factor of 3.5×10^{-3} lower than for polycrystalline material or for our eutectic with a large volume concentration of interfaces. For these alterations, but for all other factors remaining the same we determine a steady state creep expression for sapphire crystals of [0 0 0 1] orientation at 1400 °C which is shown as the dashed line in Fig. 5, confirming our expectation of a lower creep resistance in comparison with the Al_2O_3/c-ZrO_2 eutectic.

The creep model we presented is based on the existing evidence of the measured creep rates, their stress and temperature dependence and on the findings of the earlier work of Firestone and Heuer[3] on single crystal sapphire. However, the work leaves many unanswered questions. Foremost among these are the details of the continuance of the all-important fluxes of climbing dislocations, their origins, their form of maintenance and the fine structure of cores of dislocations such as details of jogs where the actual climb steps occur by O ion vacancy emission. Preliminary energetic considerations of dislocation emission from ledges on the ubiquitous interfaces or from misfit dislocations along interfaces have indicated very large energy barriers under the prevailing local stresses. However, other forms of heterogeneous nucleation of dislocations from interfaces must still be considered. Other possibilities for inelastic behavior such as Coble creep were discounted because of the apparent general absence of transverse boundaries in the topologically continuous Al_2O_3 component and the generally linear stress dependence of creep flow by this mechanism, which if present, appears to be swamped by dislocation climb flow. Parenthetically, it should be quite likely that the encapsulated c-ZrO_2 components can undergo stress relaxation entirely by diffusional Coble flow along its interfaces with the Al_2O_3 component, but in the absence of transverse grain boundaries in the Al_2O_3, that topologically continuous component can elongate only by dislocation fluxes by climb. Other possible mechanisms as well as the missing details of the maintenance of climb fluxes of dislocations could come from TEM studies which are now in progress, and would be reported elsewhere.

6. Conclusions

(1) In the eutectic of Al_2O_3/c-$ZrO_2(Y_2O_3)$ the majority phase of Al_2O_3 is topologically continuous, has a nearly perfect texture of [0 0 0 1] parallel to the growth direction and encapsulates everywhere the minority c-ZrO_2 phase which itself has a growth texture of ⟨1 1 2⟩.
(2) The interfaces separating the phases are well structured but are incoherent over most of the area.
(3) A large fraction of the c-ZrO_2 phase has a sub-micron oriented fibrillar or plate-like morphology which often, but not always, aggregates into colonies. The remaining fraction, usually surrounding the colonies of oriented fibrils or platelets is of a coarser, micron size.
(4) Upon first application of stress, transient creep is observed which is attributed to stress relaxation in the coarser fraction of the c-ZrO_2. The sub-micron fraction is considered to be too small to undergo deformation by crystal plasticity and is expected to be dormant.
(5) In steady state creep, stress changes do not produce additional transients within the resolution of stress measurements.
(6) The stress dependence of the steady state creep rate is of power-law form with an exponent in the range between 4.5 to 5.0. The activation energy of the creep rate is 71.1 kcal/mol in the 1400–1500 °C range and is attributed to oxygen ion diffusion through the Al_2O_3 and along the interfaces.
(7) Because of the [0 0 0 1] texture of the Al_2O_3 phase which must control the overall creep rate for topological reasons, the proposed steady state model is based on the climb of the $(1/3)\langle\bar{1}101\rangle$ dislocations in Al_2O_3 since the latter are sessile in glide.
(8) In the creep model which is a generallization of the steady state diffusional creep model of Nabarro,[19] the stress exponents of larger than 3 are attributed to the necessity of repeated bowing and straightening of the climbing dislocations in Al_2O_3 as they circumvent the sub-micron c-ZrO_2 domains.

(9) The predictions of the creep model, which has no adjustable constants, agree quite well with experimental observations.
(10) Finally, a mechanistic comparison of the creep resistance of the Al_2O_3/c-$ZrO_2(Y_2O_3)$ eutectic with that of [0 0 0 1] sapphire single crystal indicates that the former appears superior because of the obstructions of the dispersoid-like c-ZrO_2 domains to the the climbing dislocations of the Al_2O_3 phase, even though the diffusion constant of sapphire single crystals is three orders of magnitude smaller than that of the eutectic.

Acknowledgements

This research has been supported by the AFOSR under grant F49620-99-0276. Support for equipment development and for some other research expenses was also derived from the former Quentin Berg Professorship Fund of the Department of Mechanical Engineering, as well as other Departmental funds.

Appendix A. The kinematics of creep strain rate by climb

As presented in Section 4.2, if a single set of parallel edge dislocations of density ρ were to climb with a velocity v_c, a strain rate $\dot{\varepsilon}_0 = b\rho v_c$ would result in the direction perpendicular to the plane of the climbing dislocations.

Referring now to Fig. 8, consider the coordinate axis set 1, 2, 3 of a pyramidal glide system in a round bar of Al_2O_3 where the 1 axis is parallel to the Burgers vector of the pyramidal edge dislocations and the 1, 3 pyramidal plane makes an angle ϕ with respect to the bar axis z. Under a tensile stress σ_1 then, a density ρ of dislocations climbing in the 2 direction (positive edge dislocations in the negative 2 direction and negative edge dislocations in the positive 2 direction) a creep rate $\dot{\varepsilon}_0$ in the 1 direction of would result. However, such climb requires extension of extra half planes which requires material fluxes to arrive to the dislocation from all directions and dispersal of vacancies into all directions, resulting in contractile strain rates $\dot{\varepsilon}_{1c}, \dot{\varepsilon}_{2c}, \dot{\varepsilon}_{3c}$. For preservation of volume, it would be necessary that

$$\dot{\varepsilon}_0 + \dot{\varepsilon}_{1c} + \dot{\varepsilon}_{2c} + \dot{\varepsilon}_{3c} = 0 \tag{A.1}$$

and since by symmetry

$$\dot{\varepsilon}_{1c} = \dot{\varepsilon}_{2c} = \dot{\varepsilon}_{3c} \tag{A.2}$$

we have net strain rates

$$\dot{\varepsilon}_1 = \frac{2}{3}\dot{\varepsilon}_0 \tag{A.3a}$$

and

$$\dot{\varepsilon}_2 = \dot{\varepsilon}_3 = -\frac{1}{3}\dot{\varepsilon}_0 \tag{A.3b}$$

Resolving these strain rates into the axes r, and z of the creep bar we have

$$\dot{\varepsilon}_z = \left(\frac{2}{3} - \cos^2\,\phi\right)\dot{\varepsilon}_0 \tag{A.4a}$$

$$\therefore \dot{\varepsilon}_r = -\left(\frac{1}{3} - \frac{1}{2}\cos^2\,\phi\right)\dot{\varepsilon}_0 \tag{A.4b}$$

Since there are three sets of pyramidal dislocations, all with equal capacity to contribute to axial strain rate, we take the total axial strain rate to be

$$\dot{\varepsilon}_z = (2 - 3\cos^2\,\phi)\dot{\varepsilon}_0 \tag{A.5a}$$

and

$$\dot{\varepsilon}_r = -\left(1 - \frac{3}{2}\cos^2\,\phi\right)\dot{\varepsilon}_0 \tag{A.5b}$$

where the dislocation velocity in $\dot{\varepsilon}_0$ is still related to tensile stresses parallel to the Burgers vectors of the pyramidal dislocations. Resolving these tensile stresses to the axial tensile stress σ_z, then gives the climb-causing tensile stresses

$$\sigma_1 = q\sigma_z(1 - \cos^2\,\phi) \tag{A.6}$$

where the factor q, which needs to be determined from a FEM boundary value problem, refers to the volume average of the climb producing stress in the Al_2O_3 component between the c-ZrO_2 components. This development is discussed in Section 4.3.

References

1. Fleischer, R. L., High strength, high temperature intermetallic compounds. *J. Mater. Sci.*, 1987, **22**, 2281–2288.
2. Sayir, A. and Farmer, S. C., The effect of microstructure on mechanical properties of directionally solidified $Al_2O_3/ZrO_2(Y_2O_3)$ eutectic. *Acta Mater.*, 2000, **48**, 4691–4697.
3. Firestone, R. F. and Heuer, A. H., Creep deformation of 0° degree sapphire. *J. Am. Ceram. Soc.*, 1976, **59**, 24–29.
4. Chiang, J., Bodur, C. T. and Argon, A. S., Pyramidal edge dislocation cores in sapphire. *Phil. Mag. Lett.*, 2003, **83**, 659–666.
5. Bodur, C. T., Chiang, J. and Argon, A. S., Molecular dynamics simulations of basal and pyramidal system edge dislocation cores in sapphire. *J. Eur. Ceram. Soc.*, 2005, **25**, 1431–1439.
6. Edelin, G. and Poirier, J. P., A study of dislocation climb by means of diffusional creep experiments in magnesium. I. Deformation mechanism. *Phil. Mag.*, 1973, **28**, 1203–1210 [in French].
7. Morgan, P.-E.-D. and Marshall, D. B., Ceramic composites of monazite and alumina. *J. Am. Ceram. Soc.*, 1995, **78**, 1553–1563.
8. Lev, L. C. and Argon, A. S., Oxide-fiber/oxide-matrix composites. *Mater. Sci. Eng.*, 1995, **A195**, 251–261.
9. Sayir, A., Directional solidification of eutectic ceramics. Unpublished report (NASA Glenn Research Center, private communication).
10. Fraser, C. S., Dickey, E. C. and Sayir, A., Crystallographic texture and orientation variants in $Al_2O_3/Y_3Al_5O_{12}$ directionally solidified eutectic crystals. *J. Cryst. Growth*, 2001, **233**, 187–195.

11. Yi, J., Creep Resistance of Directionally Solidified Eutectic Ceramic: Experiments and Models PhD Thesis, Mech. Eng. Dept. M.I.T., 2004.
12. Pastor, J. Y., Poza, P., Llorca, J., Pena, J. I., Merino, R. I. and Orera, V. M., Mechanical properties of directionally solidified $Al_2O_3/ZrO_2(Y_2O_3)$ eutectics. *Mater. Sci. Eng.*, 2001, **A308**, 241–249.
13. Mazerolles, L., Michol, D. and Portier, R., Interfaces in oriented $Al_2O_3/ZrO_2(Y_2O_3)$ eutecitcs. *J. Am. Ceram. Soc.*, 1986, **69**, 252–255.
14. Dickey, E. C., Frazer, C. S., Watkins, T. R. and Hubbard, C. R., Residual stresses in high temperature ceramic eutectics. *J. Eur. Ceram. Soc.*, 1999, **19**(13–14), 2503–2509.
15. Messerschmidt, U., Baufeld, B. and Baither, D., Plastic deformation of cubic zirconia single crystals. *Key Eng. Mater.*, 1998, **153–154**, 143–182.
16. Wolfenden, A., Measurement and analysis of elastic and anelastic properties of alumina and silicon carbide. *J. Mater. Sci.*, 1997, **32**, 2275–2282.
17. Argon, A. S., Yi, J. and Sayir, A., Creep resistance of directionally solidified ceramic eutectics of Al_2O_3/c-ZrO_2 with sub-micron columnar morphologies. *Mater. Sci. Eng.*, 2001, **A319–321**, 838–842.
18. Pollock, T. M. and Argon, A. S., Creep resistance of CMSX-3 nickel base superalloy single crystals. *Acta Metall.*, 1992, **40**, 1–30.
19. Nabarro, F. R. N., Steady state diffusional creep. *Phil. Mag.*, 1967, **16**, 231–238.
20. Li, J. C. M., Kinetics and dynamics in dislocation plasticity. In *Dislocation Dynamics*, ed. A. R. Rosenfield, G. T. Hahn, A. L. Bement and R. I. Jaffee Jr. McGraw-Hill, New York, 1968, pp. 87–116.
21. Bardeen, J. and Herring, C., Diffusion in alloys and the Kirkendall effect. In *Imperfections in Nearly Perfect Crystals*, ed. W. Shockley, J. H. Hollomon, R. Maurer and F. Seitz. John Wiley & Sons, NY, 1952, pp. 261–288.
22. Brown, L. M. and Stobbs, W. M., Modeling structural changes in deformed dispersion strengthened crystals. In *Constitutive Equations in Plasticity*, ed. A. S. Argon. M.I.T. Press, Cambridge, MA, 1975, pp. 387–429.
23. Friedel, J., *Dislocations*. Addison-Wesley, Reading, MA, 1964, p. 104.
24. Groves, G. W. and Kelly, A., Change of shape due to dislocation climb. *Phil. Mag.*, 1969, **19**, 977–986.
25. Oishi, Y. and Kingery, W. D., Self-diffusion of oxygen in single crystal and polycrystalline aluminum oxide. *J. Chem. Phys.*, 1960, **33**, 480–486.